Modelling the redox imbalance in Dominant Optic Atrophy: the case of respiratory Complex I

Nadège Merabet, Joël Bordeneuve-Guibé, Noélie Davezac

Modelling the redox imbalance in Dominant Optic Atrophy: the case of respiratory Complex I ⋆

Nadège Merabet, [*,**] **Joël Bordeneuve,** [*,***]
Noélie Davezac, [**]

[*] *ISAE-Supaéro, Toulouse University, Toulouse, France*
[**] *Research Center on Animal Cognition (CRCA), Toulouse University, CNRS, UPS, Toulouse, France*
[***] *Corresponding author: joel.bordeneuve@isae.fr*

Abstract: Dominant Optic Atrophy is a neuro-ophthalmic disease characterized by the degeneration of the optic nerves. As other neurodegenerative diseases, this pathology was associated with dysfunctional mitochondrial respiratory complexes and an increased production of Reactive Oxygen Species (ROS). Our objective is to create a mathematical model of the molecular mechanisms involved in the pathogenesis of Dominant Optic Atrophy in order to predict their evolution and give appropriated treatment based on *in-silico* analysis with physiological parameters from a specific patient. The first part of the work presented here concerns processes and feedback mechanisms of the whole dysfunctional mitochondrial system. The behaviour of the system is explained with a block diagram. In the second part, we present a detailed stochastic model of catalytic activity and ROS production of respiratory complex I. We developed the model using a Petri net formalism and a continuous-time Markov chains theory. The simulations were realized on Matlab and compared to kinetic data from the literature. Our model is able to reproduce the dynamics of the complex I system and to simulate observed behaviours of this system regarding ROS production.

Keywords: Biological systems; Computer simulation; Markov models; Stochastic Petri-nets; Stochastic modelling

INTRODUCTION

Neurodegenerative diseases are a major issue of public health. Among these pathologies, neuro-ophthalmic conditions including glaucoma, which affects 80 millions of patients worldwide, but also genetic neurodegeneration of the retina as in Dominant Optic Atrophy (DOA), are central questions of our societies. Although mutations in the nuclear gene OPA1 have been identified as the main cause of DOA, the physio-pathological mechanisms involved are still unknown and there is no therapy to date.

DOA is characterized by moderate to severe loss of visual acuity with insidious onset in early childhood. The disease primarily affects the retinal ganglionic cells (RGC) resulting in optic nerve atrophy. There is a considerable inter- and intra-familial variation in visual acuity (Votruba et al., 1998), and the penetrance may be as low as about 40% (Toomes et al., 2001). Estimated disease prevalence is between 1:10,000 in Denmark and 1:50,000 worldwide. The majority of patients (about 75%) with DOA harbors mutation in the OPA1 gene (Delettre et al., 2000) which usually results in the reduction in OPA1 protein levels. Interestingly, recent studies evidenced a severe multi-systemic disorder associated with some OPA1 mutations, named DOA plus syndrome (Amati-Bonneau et al., 2008). Patients present additional neurological complications in adult life, including ataxia, sensorineural deafness, chronic progressive external ophtalmoplegia, sensorymotor neuropathy and myopathy . These observations are of major pathophysiological importance, highlighting the widespread deleterious consequences of OPA1 mutations, not only for RGCs, but also for other neuronal populations and skeletal muscle. Glaucoma was also clearly related to OPA1 gene status (Ju et al., 2010) with patients presenting downregulation of its expression (Bosley et al., 2011).

The OPA1 gene encodes a mitochondrial protein localized in the inter-membrane space and anchored to mitochondrial inner membrane which has various functions, including inner membrane fusion, cristae structuration, mtDNA maintenance, protection from apoptosis and mitochondrial energetics modulation (Landes et al., 2010). The general impact of OPA1 inactivation on mitochondrial energetics modulation was investigated by Bertholet et al. and Millet et al. in cellular models (rat cortical neurons and HeLa cells), in $OPA1^{enu/+}$ mice and in fibroblasts from DOA and DOA+ patients. In both cellular models (HeLa cells and cortical neurons), complex I, complex III and complex IV are impaired and cellular respiration is diminished when OPA1 is decreased (Bertholet et al., 2013). This

⋆ This project is supported by grants from the Centre National de la Recherche Scientifique, the Université Paul Sabatier and, the Région Occitanie. N. Merabet is funded by the French Ministry for Research and Education and the Ecole Doctorale Aéronautique Astronautique for Ph.D. studies.

is accompanied by an increase in mitochondrial Reactive Oxygen Species (ROS) production, which is buffered by the activation of antioxidant defences. However, this situation leads to a pro-oxidative state, since further acute or chronic exogenous oxidative stress challenged both the antioxidant response and the viability of OPA1 depleted neurons. Interestingly, some patients showed altered expression of genes implicated in the antioxidant machinery (Millet et al., 2016). The authors proposed that mutations or decreased quantity of OPA1 induce an imbalance in the cellular redox state, weakening cells to exogenous pro-oxidative stresses and leading to late onset apoptotic death, that thus could be prevented.

Our objective is to create a mathematical model of the molecular mechanisms involved in Dominant Optic Atrophy (DOA) and glaucoma, based on these assumptions, in order to predict their evolution and give appropriated treatment based on *in-silico* analysis with physiological parameters for a specific patient. This paper is divided into three sections and a conclusion. The first part provides a description of the hypothesized molecular mechanisms and the components to consider in the model. The second part focuses on the ROS production of mammalian complex I. The third part describes the model and techniques we used to model complex I and the first results. Finally, the ongoing work will be outlined in the conclusion.

1. SYSTEM MODEL OF MITOCHONDRIAL (DYS)FUNCTIONS

Mitochondrial processes are central to the control of overall cell metabolism. However, the large number of interacting reactions and pathways involving mitochondrial subsystems together with limited experimental observations makes it very challenging to understand and model the dynamics of this complex system. For this reason, we used a block diagram to describe the possible behaviour of this system in the context of DOA (fig.1). This formalism aims at determining which processes and subsystems are of interest in developing a better understanding of system interactions and creating a model of DOA molecular mechanisms.

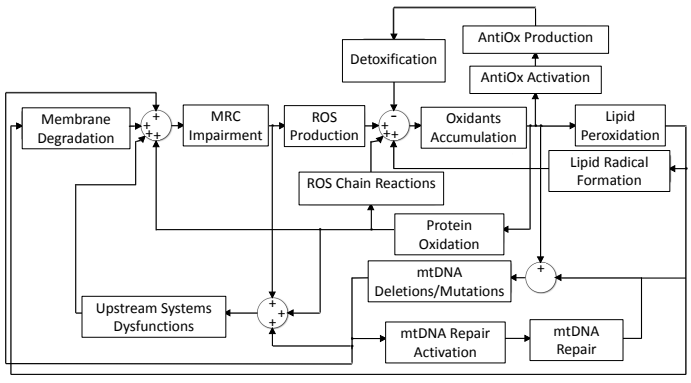

Fig. 1. Block diagram of mitochondrial systems interactions in Dominant Optic Atrophy. MRC, Mitochondrial Respiratory Chain; ROS, Reactive Oxygen Species; AntiOx, Antioxidants; mtDNA, mitochondrial DNA.

The oxidative phosphorylation is an essential part of the mitochondrial energetic metabolism. It consists of five enzyme complexes that are located in the inner mitochondrial membrane. Four of them (complexes I-IV) compose the mitochondrial respiratory chain (MRC) or electron transport chain whose function is to establish an electrochemical proton gradient over this membrane and the fifth complex, the F1Fo-ATPsynthase uses the force of this gradient for the phosphorylation of adenosin-diphosphate (ADP) to adenosin-triphosphate (ATP).

During a normal function of the MRC, ROS are basically produced essentially by the first and third complexes. However, complex I and complex III dysfunctions, caused by genetic, environmental and pathological factors result in a dramatic increase of their production of ROS.

ROS production by the dysfunctional respiratory chain and their deleterious consequences are described in our block diagram (fig.1).

These consequences comprise:

- protein oxidation (Stadman and Levine, 2000);
- lipid peroxidation (Halliwell and Chirico, 1993);
- mitochondrial DNA (mtDNA) mutations and deletions (Richter et al., 1988).

All these processes result in a further dysfunction of the MRC leading to reinforcing feedback loops, contributing to cell death, that correspond to positive feedback loops on the block diagram (fig.1):

- Respiratory complexes and proteins linked to their well functioning are affected by mechanisms of protein oxidation induced by ROS (Stadman and Levine, 2000);
- Lipid peroxidation has two consequences: structural damage to membranes affecting the function of membrane proteins including the MRC and generation of secondary products. These products exhibit high reactivity with proteins, mtDNA and lipids (Repetto et al., 2010)
- The mtDNA encoded genes include seven subunits of complex I, one subunit of complex III, three subunits of complex IV and two subunits of complex V (Schon et al., 2012). Therefore, accumulating mtDNA mutations result in a decreased activity of the MRC and an increased ROS production.

These deleterious consequences can be minimized under the action of mtDNA repairing enzymes (Kazak et al., 2012) and ROS scavengers, including enzymes and quenchers (Halliwell and Gutteridge, 1999). These balancing actions correspond to the two negative feedback loops of the block diagram (fig.1). However, these balancing actions have a limited extent as Millet et al. observed in the context of DOA (Millet et al., 2016) and can be saturated.

We first focused on the production of ROS by the MRC in the development of our model and more particularly on Complex I. ROS are derived from molecular oxygen and superoxide anion $O_2^{\cdot-}$, the product of a one-electron reduction of oxygen is the precursor of most ROS (Turrens, 2003). Complex I appears to be the primary source of $O_2^{\cdot-}$ in the brain under normal conditions and in a variety of

pathological scenarios ranging from ageing to Parkinson's disease (Turrens, 2003).

2. COMPLEX I MECHANISMS

2.1 Structure and function

The role of Complex I is to oxidize NADH to NAD^+, reduce ubiquinone (Q) to ubiquinol (QH2) and translocate four protons across the inner membrane of the mitochondria to create a proton-motive force. Complex I from *Bos Taurus* heart mitochondria is the most studied mammalian complex I (Hirst and Roessler, 2016) and comprises 45 proteins among which 14 conserved 'core' units are sufficient to catalyse energy transduction (Fiedorczuk et al., 2016). These 14 subunits are divided into a hydrophilic redox domain and a hydrophobic domain contained in the mitochondrial inner membrane (fig.2) and involved in protons translocation (Fiedorczuk et al., 2016).

NADH is oxidized by a non-covalently bound flavin mononucleotide (FMN) at the top of the hydrophilic domain. It almost certainly occurs by hydride transfer (single step transfer of 2 electrons and one proton from NADH to FMN) (Hirst and Roessler, 2016).

The fully reduced flavin $FMNH^-$ and the semi-reduced flavin $FMNH^{\cdot}$ transfer these electrons one by one to a chain of eight ironsulfur (FeS) clusters constituting the redox centers of the Complex I. The last cluster of the chain is the electron donor to the Q-binding site. It is generally accepted that biological electron transfer is a process of tunnelling (Moser et al., 1992). Electron paramagnetic resonance (EPR) studies on complex I from *Bos taurus* revealed an alternating profile of higher and lower potential clusters (Bridges et al., 2012). The alternating potentials could contribute to the fast transfer of electrons and act as a dynamic waiting queue for electrons, to synchronize the different processes occurring in the complex I.

2.2 ROS production

Kinetic studies showed that the fully reduced flavin is the electron donor to molecular oxygen and that an increase in NADH concentration induces an increase of ROS production (Kussmaul and Hirst, 2006), while a further increase in NADH buffers this ROS production (Birrell et al., 2009). NAD^+ inhibits ROS production even at low concentrations. Finally, while quinol favours the increase in ROS due to a blockage of complex I, addition of quinone buffers it (Kussmaul and Hirst, 2006).

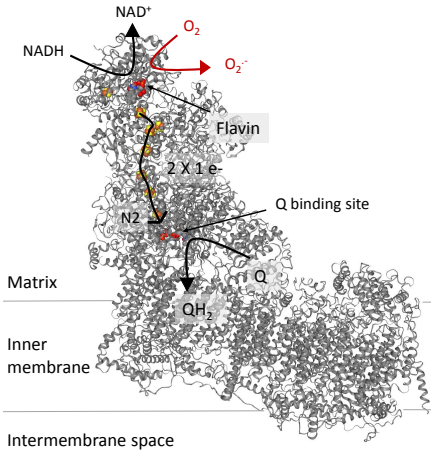

Fig. 2. Complex I mechanism. Adapted from (Vinothkumar et al., 2014)

2.3 Existing models and their limits

Black box models of complex I failed to describe its functioning. Indeed, recently, it was shown that the kinetics of Complex I do not obey a ping-pong mechanism as it was assumed to, due to a strong spatial separation of NADH oxidation and Q reduction and the presence of the iron-sulfur cluster chain between NADH- and Q-binding sites (Ransac et al., 2012). Electrons do not simply transfer across the chain but jump back and forth depending on the states of the closest redox centres and the probability of electrons tunnelling.

A detailed stochastic model of complex I was consequently proposed (Ransac et al., 2012). However, this model does not simulate the production of ROS by Complex I. Moreover, the alternating profile of potentials observed in mammalian complex I (Bridges et al., 2012) was not considered for the calculations of electron tunnelling probabilities between iron-sulfur clusters. In addition, the probability of reverse transfer between flavin and NAD^+ might have been overestimated: all the steps of the simulations were used by the electrons exchange between the flavin and $NADH/NAD^+$. Besides it is likely that the interconversion of NADH and NAD^+ is thermodynamically not reversible. It requires the application of an important driving force. Finally, only the binding constants of the substrates were adjusted and with limited kinetic data regarding the effects of the different substrates on Complex I activity.

In contrast, we propose a detailed stochastic model of Complex I which:

- includes the alternating profile of iron-sulfur clusters potentials
- considers a non thermodynamical reversibility of the hybrid electron proton transfer from NADH to the flavin
- includes ROS production by Complex I in the form of $O_2^{\cdot-}$.

3. COMPLEX I MODEL

We modelled the complex I as a stochastic Petri net (SPN), taking into account the alternating profile of potentials of the iron-sulfur clusters and a reasonable rate for the reverse reaction between FMN and NADH to estimate the transition probabilities and we simulated the net using a Gillespie algorithm.

3.1 Petri net modelling description

The Petri net modelling the redox mechanism of Complex I is represented in fig.3. It is composed of 11 places which can contain the number of tokens indicated between brackets. The tokens represent the electrons. The places whose name start with N correspond to the iron-sulfur clusters. Cluster

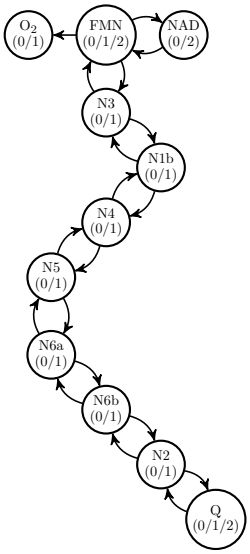

Fig. 3. Petri net model of Complex I

N1a is not included in the model since it cannot be reduced by NADH (Bridges et al., 2012).

To simulate the net, we consider an equivalence between the different number of tokens a place can contain and the associated set of different chemical species. For instance, the flavin place can contain 0, 1 or 2 electrons: this respectively corresponds to the oxidized flavin FMN, the semi-reduced flavin $FMNH^{\cdot}$ and the fully reduced flavin $FMNH^{-}$.

The objective is to simulate evolution of their respective number of molecules. The numbers of molecules of the substrates and of O_2^- are not constrained. In contrast, the other species can be represented only by one or zero copy since there are only one of each cluster and one flavin center in one complex I. Moreover, they cannot coexist: for instance we have N5 or $N5^-$ for a given state of the system but we cannot have both at the same time. We assume that the semiquinone SQ which is the intermediate between the first step and the second step of Q reduction does not dissociate and hence can exist in only one copy. We also take into account the binding and dissociation of the substrates and consider that the protons translocation occurs simultaneously with the reduction of Q.

We note the vector of different chemical species $[S_1, ..., S_N]$ and the vector of their respective number of molecules $[X_1, ..., X_N]$. The firing of a transition corresponds to a chemical reaction: the weights of the Petri net are therefore determined by the stoichiometry of the reaction taking place during the corresponding transition. We note the vector of reaction channels $[R_1, ..., R_M]$.

3.2 Probability rate constants calculation

We use the formalism proposed by Gillespie in his construction of a stochastic simulation algorithm for chemical systems (Gillespie, 1992) and note $\Pi_\mu(t, dt)$ the probability that a randomly selected combination of R_μ, reactant molecules at time t will react accordingly in the next infinitesimal time interval $[t, t + dt)$. Biological electron transfers fall within a context in which this probability can be modelled as linearly dependent on dt (Moser and Dutton, 1996; Gillespie, 1994). For each reaction channel R_μ:

$$\Pi_\mu = c_\mu dt \tag{1}$$

where c_μ is independent of dt. We call c_μ the probability rate constant for reaction channel R_μ.

Based on experimental measurements and the Marcus theory of electron transfer, Moser et al. (Moser et al., 1992) derived an empirical relation between the rate of exergonic intraprotein electron transfer and the spatial separation between electron donor and acceptor, which has proved to be successful for distances above 4 Å (Moser et al., 2008):

$$\log(k_{exer}) = 15 - 0.6D - 3.1\frac{(\Delta G + \lambda)^2}{\lambda} \tag{2}$$

Where, D is the edge-to-edge donor-acceptor distance in Å, ΔG is the driving force of the reaction in eV and λ is the the reorganization energy required to change the nuclear coordinates upon electron transfer. For endergonic reactions they proposed a penalty term (Page et al., 1999) (ΔG is negative for an exergonic reaction):

$$\log(k_{ender}) = \log(k_{exer}) + \frac{\Delta G}{0.06} \tag{3}$$

The values for the driving forces are approximated using the differences of potentials measured in EPR studies (Bridges et al., 2012). The values for the distances are taken from crystallographic studies(Fiedorczuk et al., 2016). Finally, we used the value $\lambda = 0.7$ eV proposed by Moser et al. on an empirical basis (Moser et al., 1992).

Concerning the reaction between NADH and the flavin, it involves the transfer of a proton which is nearly 2000 times heavier than an electron and occurs at a distance inferior to 4 Å. For this reason we do not use the previous relations to estimate this probability rate. We assume that the proton transfer will be the limiting aspect of this transfer and estimate its rate by calculating its velocity under the acceleration of the electric field created by the chemical species and multiplying it by the distance between NADH and FMN. The electrical field is assumed to be constant and estimated considering the difference of potentials between the two species and a distance of 3.2 Å (Berrisford and Sazanov, 2009) between the flavin and NADH. The value used for proton mobility is $3.2 * 10^{-3}$ $cm^2.V^{-1}.s^{-1}$. The rate obtained is of order 10^{12} s^{-1}.

We assume that the reverse transfer is possible but only under the application of an external driving force: under normal conditions, the local conformation around the flavin could be modified in the presence of NADH and not NAD^+ (observed on bacterial complex I (Mamedova et al., 2004)). For this reason the rate of the reverse inverse is very small compared to the rate of forward transfer (of order $10^2 - 10^3$). We applied the same reasoning to the reversibility of transfer between N2, this time for probable local conformational changes under proton translocation and protonation of Q.

3.3 Simulation algorithm

The linear-dt transition probabilities of the model allow to simulate the SPN model of complex through its underlying Continous-Time Markov Chain and to use the Gillespie algorithm to this purpose (Gillespie, 1992).

We consider: $h_\mu(n_1, ..., n_n)$ the number of distinct combinations of R_μ reactant molecules at time t when there are exactly n_i of the S_i molecules; and $p(\tau, \mu/\mathbf{n}, t)d\tau$ the probability that, given $\mathbf{X}(t) = \mathbf{n}$, the next reaction in the system will occur in the infinitesimal time interval $[t + \tau, t + \tau + d\tau)$, and will be an R_μ reaction. It can be shown (Gillespie, 1992) that:

$$p(\tau, \mu/\mathbf{n}, t) = a(\mathbf{n}) \exp(-a(\mathbf{n})\tau) \frac{c_\mu h_\mu(\mathbf{n})}{a(\mathbf{n})} \quad (4)$$

where $a(\mathbf{n}) = \sum_{\mu=1}^{N} c_\mu h_\mu(\mathbf{n})$.

Given $\mathbf{X}(t) = \mathbf{n}$, the 'time to the next reaction' and the 'index of the next reaction' are statistically independent random variables, the former having the exponential density function with decay constant $a(\mathbf{n})$, and the latter having the integer density function $\frac{c_\mu h_\mu(\mathbf{n})}{a(\mathbf{n})}$.

It can be shown (Gillespie, 1992) that we can generate a statistically exact sample pair (τ, μ) according to this joint density function by first generating two unit-interval uniform random numbers r_1 and r_2, then taking τ to be:

$$\tau = \frac{1}{a(\mathbf{n})} \ln(\frac{1}{r_1}) \quad (5)$$

and taking μ to be the smallest integer for which:

$$\sum_{m=1}^{\mu} c_m h_m(\mathbf{n}) > r_2 a(\mathbf{n}) \quad (6)$$

Finally, the algorithm used to simulate the Petri net takes the following form (Gillespie, 1977):

1: Input the desired values for the M reaction constants $[c_1, ..., c_M]$ and the N initial molecular population numbers $[X_1, ..., X_N]$. Set t_{max}, $t = 0$.
2: **while** $t \leq t_{max}$ **do**
3: Calculate and store $a_\mu = h_\mu c_\mu$ for $\mu = 1, ..., M$ and $a_0 = \sum_{\mu=1}^{M} a_\mu$.
4: Generate two random numbers r_1 and r_2, using a unit-interval uniform random number generator, and calculate (τ, μ) based on equations 5 and 6 .
5: Adjust X_i to reflect the occurrence of the R_μ reaction.
6: Put $t = t + \tau$.
7: **end while**

3.4 Comparison to experimental data

The fixed parameters in the relationships derived by Moser et al. (Moser et al., 1992) are average parameters for redox proteins (Page et al., 1999). We first considered other possible fixed parameters values and used a tabu search algorithm for the binding and dissociation constants, to fit the results of our numerical simulations with experimental data from the literature (Sherwood and Hirst, 2006). Then we fitted the value of the probability rate constant for $O_2^{\cdot-}$ formation using data from (Kussmaul and Hirst, 2006).

4. RESULTS

Fig.4a shows the simulated reduction of 100 µM Q by 100 µM NADH catalysed by 15 mg.ml^{-1} Complex I without O_2 compared to experimental data in (Sherwood and Hirst, 2006). Fig.4b and fig.4c show the simulated dependence of $O_2^{\cdot-}$ production on [NADH] compared to experimental data in (Kussmaul and Hirst, 2006). At low concentrations of NADH the rate of $O_2^{\cdot-}$ is almost independent of NADH with a very slight increase until 3 µM of NADH. At higher concentrations NADH exerts an inhibitory effect on $O_2^{\cdot-}$ production. Fig.4d shows the simulated linear dependence of $O_2^{\cdot-}$ production on O_2 concentration (% saturated in air) at 30 µM NADH compared to experimental data in (Kussmaul and Hirst, 2006).

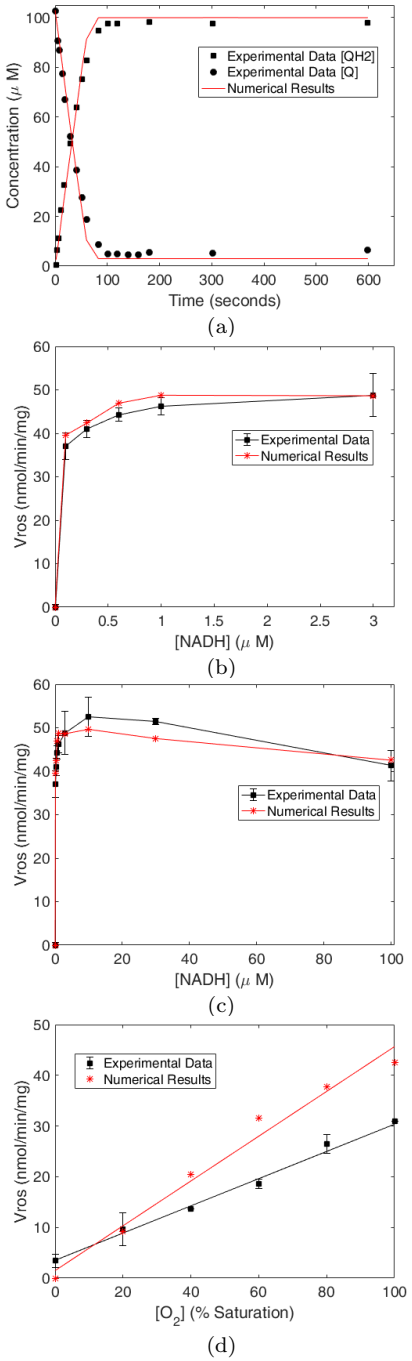

Fig. 4. Computer simulations of Complex I catalytic activity and ROS production compared to experimental data taken from (Sherwood and Hirst, 2006) and (Kussmaul and Hirst, 2006). In (b) to (d) Vros stands for the rate of formation of $O_2^{\cdot-}$ in nmol/min/mg of Complex I.

5. DISCUSSION

We have developed a stochastic model able to reproduce the dynamics of mitochondrial complex I and to simulate its production of $O_2^{\cdot-}$ under certain conditions . However, measurements of $O_2^{\cdot-}$ concentrations are usually done using indirect methods and, are prone to uncertainty and a high variability. For instance, the approximate rate measured in fig.4c at 30 µM NADH and 100% O_2 saturation is different from the rate measured in fig.4d under the same conditions (respectively 50 nmol/min/mg and 30 nmol/min/mg). The value of the probability rate constant for $O_2^{\cdot-}$ formation was fitted using data in fig.4c which explains the distance between numerical and experimental data on fig.4d. This highlights the need to incorporate uncertainty in our model in order to reach our long term objective which is to create a mathematical model of DOA able to predict the evolution of the disease for a specific patient and to give a personalized treatment.

ACKNOWLEDGEMENTS

We thank Jérôme Morio for helpful discussion.

REFERENCES

Amati-Bonneau, P. et al. (2008). Opa1 mutations induce mitochondrial dna instability and optic atrophy 'plus' phenotypes. *Brain*, 131(2), 338–351.

Berrisford, J.M. and Sazanov, L.A. (2009). Structural basis for the mechanism of respiratory complex i. *J. Biol. Chem*, 284(43), 29773–29783.

Bertholet, A.M. et al. (2013). Opa1 loss of function affects in vitro neuronal maturation. *Brain*, 136(5), 1518–1533.

Birrell, J.A. et al. (2009). Reactions of the flavin mononucleotide in complex i: A combined mechanism describes nadh oxidation coupled to the reduction of apad+, ferricyanide, or molecular oxygen. *Biochemistry*, 48(50), 12005–12013.

Bosley, T.M. et al. (2011). Down-regulation of opa1 in patients with primary open angle glaucoma. *Mol. Vis*, 17, 10741079.

Bridges, H.R., Bill, E., and Hirst, J. (2012). Mössbauer spectroscopy on respiratory complex i: The ironsulfur cluster ensemble in the nadh-reduced enzyme is partially oxidized. *Biochemistry*, 51(1), 149–158.

Delettre, C. et al. (2000). Nuclear gene opa1, encoding a mitochondrial dynamin-related protein, is mutated in dominant optic atrophy. *Nat. Genet*, 26(2), 207210.

Fiedorczuk, K. et al. (2016). Atomic structure of the entire mammalian mitochondrial complex i. *Nature*.

Gillespie, D.T. (1977). Exact stochastic simulation of coupled chemical reactions. *The Journal of Physical Chemistry*, 81(25), 2340–2361.

Gillespie, D.T. (1992). A rigorous derivation of the chemical master equation. *Physica A: Statistical Mechanics and its Applications*, 188(1), 404 – 425.

Gillespie, D.T. (1994). Why quantum mechanics cannot be formulated as a markov process. *Phys. Rev. A*, 49, 1607–1612.

Halliwell, B. and Chirico, S. (1993). Lipid peroxidation: its mechanism, measurement, and significance. *Am J Clin Nutr*, 57(5), 715S–724S.

Halliwell, B. and Gutteridge, J.M.C. (1999). *Free Radicals in Biology and Medicine*. Oxford University Press.

Hirst, J. and Roessler, M.M. (2016). Energy conversion, redox catalysis and generation of reactive oxygen species by respiratory complex i. *BBA - Bioenergetics*, 1857(7), 872 – 883.

Ju, W.K. et al. (2010). Increased optic atrophy type 1 expression protects retinal ganglion cells in a mouse model of glaucoma. *Mol. Vis*, 16, 13311342.

Kazak, L. et al. (2012). Minimizing the damage:repair pathways keep mitochondrial dna intact. *Nat. Rev. Mol. Cell Biol*, 13, 659–671.

Kussmaul, L. and Hirst, J. (2006). The mechanism of superoxide production by nadh:ubiquinone oxidoreductase (complex i) from bovine heart mitochondria. *PNAS*, 103(20), 7607–7612.

Landes, T. et al. (2010). {OPA1} (dys)functions. *Seminars in Cell & Developmental Biology*, 21(6), 593 – 598.

Mamedova, A.A. et al. (2004). Substrate-induced conformational change in bacterial complex i. *J. Biol. Chem*, 279(22), 23830–23836.

Millet, A.M.C. et al. (2016). Loss of functional opa1 unbalances redox state: implications in dominant optic atrophy pathogenesis. *Ann Clin Transl Neurol*, 3(6), 408–421.

Moser, C.C. et al. (1992). Nature of biological electron transfer. *Nature*, 355, 796 – 802.

Moser, C.C. and Dutton, P.L. (1996). *Outline of theory of protein electron transfer*. Springer.

Moser, C.C. et al. (2008). Distance metrics for heme protein electron tunneling. *BBA - Bioenergetics*, 1777(78), 1032 – 1037.

Page, C.C. et al. (1999). Natural engineering principles of electron tunnelling in biological oxidationreduction. *Nature*, 402, 47–52.

Ransac, S. et al. (2012). From in silico to in spectro kinetics of respiratory complex i. *BBA - Bioenergetics*, 1817(10), 1958 – 1969.

Repetto, M. et al. (2010). *Lipid Peroxidation: Chemical Mechanism, Biological Implications and Analytical Determination*.

Richter, C., Park, J., and Ames, B. (1988). Normal oxidative damage to mitochondrial and nuclear dna is extensive. *PNAS*, 85(17), 64656467.

Schon, E.A. et al. (2012). Human mitochondrial dna: roles of inherited and somatic mutations. *Nat. Rev. Genet*, 13, 878–890.

Sherwood, S. and Hirst, J. (2006). Investigation of the mechanism of proton translocation by nadh:ubiquinone oxidoreductase (complex i) from bovine heart mitochondria: does the enzyme operate by a q-cycle mechanism? *Biochem. J*, 400(3), 541–550.

Stadman, E.R. and Levine, R.L. (2000). Protein oxidation. *Ann N Y Acad Sci*, 899(1), 191–208.

Toomes, C. et al. (2001). Spectrum, frequency and penetrance of opa1 mutations in dominant optic atrophy.

Turrens, J.F. (2003). Mitochondrial formation of reactive oxygen species. *J. Physiol*, 552(Pt 2), 335344.

Vinothkumar, K.R. et al. (2014). Architecture of mammalian respiratory complex i.

Votruba, M. et al. (1998). Clinical features in affected individuals from 21 pedigrees with dominant optic atrophy. *Arch Ophthalmol*, 116(3), 351–358.